Nuclear Engineering and Technology 54 (2022) 3470–3477

Contents lists available at ScienceDirect

Nuclear Engineering and Technology

journal homepage: www.elsevier.com/locate/net

Original Article

Radiation shielding properties of weathered soils: Influence of the chemical composition and granulometric fractions

Luiz F. Pires

Laboratory of Physics Applied to Soils and Environmental Sciences, Department of Physics, State University of Ponta Grossa, 84.030-040, Ponta Grossa, PR, Brazil

ARTICLE INFO

Article history:
Received 5 November 2021
Received in revised form
31 March 2022
Accepted 2 April 2022
Available online 5 April 2022

Keywords:
XCOM
Oxides
Mean free path
Half-value layer
Tenth-value layer
Mass attenuation coefficient

ABSTRACT

Soils are porous materials with high shielding capability to attenuate gamma and X-rays. The disposal of radionuclides throughout the soil profile can expose the living organisms to ionizing radiation. Thus, studies aiming to analyze the shielding properties of the soils are of particular interest for radiation shielding. Investigations on evaluating the shielding capabilities of highly weathered soils are still scarce, meaning that additional research is necessary to check their efficiency to attenuate radiation. In this study, the radiation shielding properties of contrasting soils were evaluated. The radiation interaction parameters assessed were attenuation coefficients, mean free path, and half- and tenth-value layers. At low photon energies, the photoelectric absorption contribution to the attenuation coefficient predominated, while at intermediate and high photon energies, the incoherent scattering and pair production were the dominant effects. Soils with the highest densities presented the best shielding properties, regardless of their chemical compositions. Increases in the attenuation coefficient and decreases in shielding parameters of the soils were associated with increases in clay, Fe_2O_3, Al_2O_3, and TiO_2 amounts. In addition, this paper provides a comprehensive description of the shielding properties of weathered soils showing the importance of their granulometric fractions and oxides to the attenuation of the radiation.

© 2022 Korean Nuclear Society, Published by Elsevier Korea LLC. This is an open access article under the CC BY license (http://creativecommons.org/licenses/by/4.0/).

1. Introduction

The literature shows a lot of research discussing the possible use of soil as an effective shielding material [1–4]. Yoshikawa et al. [5] presented a study in which they proposed the utilization of heavy bentonite-based slurry to shield gamma-rays and neutrons during decommissioning of the Fukushima Nuclear Power Plant. They demonstrated that gamma-ray and neutron beam reductions are directly dependent on the wet density of soil materials. Singh et al. [6] calculated the shielding effectiveness of contrasting soils by analyzing different radiation shielding parameters. They observed that all soils studied were usually suitable gamma-ray shielding materials, and the sandy loam type was considered the best neutron absorber. In a recent study, Hila et al. [7] presented a detailed analysis of the effectiveness of soil samples from the Philippine islands as a radiation shielding material. Those authors highlighted the importance of SiO_2 concentrations in soils to attenuate radiation and reported that an increase in the amount of silica resulted in a negative correlation with the effective atomic number.

Soil is a complex material composed of three phases: solid (mineral and organic matter), gases, and liquids (soil solution). The solid phase is mainly characterized by major oxides like SiO_2, Al_2O_3, Fe_2O_3, and TiO_2, among others in lower concentrations [8]. This is important due to the role of the soil oxides in the aggregation and stability of its structure, which influences the way this porous material responds to possible changes caused by the action of natural processes (water, wind, temperature, etc.) [9]. As a substantial extension of the Earth's surface is covered by soils and rocks, c. 25%, these materials become interesting for radiation shielding purposes due to their availability. However, contrasting soil compositions and densities affect differently the way the radiation interacts with this porous medium. The presence of higher atomic number elements, such as Fe_2O_3, especially in weathered soils, tends to attenuate radiation more effectively than lower atomic number elements (e.g. SiO_2), depending on the photon energy [10].

Weathered soils, commonly found in tropical climate countries,

E-mail addresses: lfpires@uepg.br, luizfpires@gmail.com.

https://doi.org/10.1016/j.net.2022.04.002
1738-5733/© 2022 Korean Nuclear Society, Published by Elsevier Korea LLC. This is an open access article under the CC BY license (http://creativecommons.org/licenses/by/4.0/).

are formed due to the hot and humid conditions to which these soils are exposed. The continuous action of temperature and moisture causes significant changes in the soil parent material throughout time. The soil mineralogy and chemical composition can be affected by tropical/sub-tropical weathering with possible consequences in their attenuation properties. Thus, monitoring the degree of weathering of this porous material and correlating it with the soil radiation interaction properties becomes a relevant matter of investigation. Indices such as Ki and Kr, which describe the molecular relationship between silicon and aluminum oxides (Ki) and the molecular relationship between silicon, aluminum, and iron oxides (Kr), can be utilized to infer the degree of soil weathering. Following Ki and Kr index calculations, the next step involves the radiation attenuation parameters calculation to access the soil shielding capabilities.

The most important parameters to evaluate the shielding properties of different materials are the linear (κ) and mass attenuation (μ) coefficients, the mean free path (λ), the half-value layer (H_{VL}), and the tenth value layer (T_{VL}) [1,11]. The linear attenuation coefficient is related to the probability of a photon being attenuated per unit of length, while λ represents the average distance between successive interactions of photons. The other two terms, H_{VL} and T_{VL}, represent the thicknesses of an absorber responsible for reducing photon intensity to half and one-tenth (decreasing the beam intensity by 90%) [11].

Nevertheless, the radiation shielding capabilities of highly weathered soils, like those found in tropical/subtropical regions, have not been studied in detail yet. Tropical soils cover a significant area of the Earth's surface (about 30 million km^2) demonstrating the importance of their characterization. Thus, this study aimed to evaluate the radiation interaction properties of contrasting soils to understand their suitability for radiation shielding. The following parameters were analyzed: κ, μ, λ, H_{VL}, and T_{VL}. The hypothesis of this study was that the clay content and heavy oxides (Fe_2O_3 + TiO_2) of weathered soils affect positively their radiation attenuation and shielding properties.

2. Material and methods

The influence of contrasting soils on the radiation attenuation shielding properties was evaluated by analyzing fifteen soils of different granulometric and chemical compositions (Table 1). Soil samples were collected at the topsoil (0–10 cm) of different municipalities in the State of Paraná, Brazil (Fig. 1a). The core idea was to evaluate the importance of soils of contrasting textures (based on clay, silt, and sand contents) and chemical compositions (oxide contents) in radiation shielding properties. The soil texture determination was based on the densimeter method with previous sample treatment (H_2O_2 30 v v^{-1}) and the use of chemical dispersion (NaOH 1.0 mol L^{-1}) [12]. According to the USDA soil texture classification system, the soils studied were classified as Clay (HC and C: 9 soils), Silt loam (SIL: 1 soil), Sandy loam (SAL: 1 soil), Clay loam (CL: 2 soils), sandy clay loam (SCL: 1 soil), and Sand (S: 1 soil) (Fig. 1b).

Table 1
Granulometric fractions (clay, silt, and sand contents) and chemical composition (major oxides) for the contrasting soil types studied.

Soil type	Granulometric fractions wt(%)			Chemical composition wt(%)			
	Clay	Silt	Sand	Al_2O_3	SiO_2	Fe_2O_3	TiO_2
HC-1	66.4	16.1	17.5	39.3	27.4	27.5	3.7
HC-2	69.3	17.8	12.9	33.5	31.5	28.9	4.1
HC-3	70.4	17.0	12.6	37.9	33.4	22.9	3.0
C-1	59.3	15.1	25.6	37.4	33.3	23.6	3.9
C-2	55.0	20.2	24.8	35.8	31.6	26.1	3.3
C-3	58.0	24.0	18.0	45.4	37.5	12.3	2.0
C-4	50.6	22.3	27.1	31.9	31.8	28.9	4.6
C-5	47.4	29.1	23.5	33.9	29.6	28.8	4.8
C-6	53.3	17.1	29.6	42.9	22.3	27.4	5.5
SIL	23.2	55.9	20.9	16.0	74.6	4.3	1.2
SAL	18.1	17.6	64.3	21.1	71.5	3.0	0.8
CL-1	37.8	27.0	35.2	24.5	58.7	12.0	3.2
CL-2	36.0	34.5	29.5	22.1	68.4	4.8	0.8
SCL	25.5	20.5	54.0	20.1	71.4	4.4	1.0
S	8.0	0.9	91.1	18.5	76.6	2.8	0.7

Major oxides comprise more than 96% of the soil chemical composition. HC: Heavy clay; C: Clay; SIL: Silt loam; SAL: Sandy loam; CL: Clay loam; SCL: Sandy clay loam; S: Sand.

Semi-quantitative elemental analysis of the soils was accomplished using the energy dispersive X-ray fluorescence (XRF) technique in the instrument model EDX-720 (Shimadzu) equipped with an Rh X-ray tube. The equipment voltage varied from 5 to 50 kV and its tube current from 1 to 1000 μA. The system detector was a Si(Li) semi-conductor cooled with liquid N at −196 °C. Details of the EDXRF analysis procedures can be found in Ferreira et al. [10].

Mass attenuation coefficient values were calculated using the XCOM computer code (Version 1.5), which gathers information from a database of attenuation coefficients [13]. This program enables μ determination for pure and compound elements or mixtures with atomic number (Z) varying from 1 to 100 in the 1 keV to 100 GeV photon energy range. The mass attenuation coefficient of a compound or mixture is given by [13]:

$$\mu = \sum_i W_i \mu_i \tag{1}$$

where μ_i is the mass attenuation coefficient of the i-th term and W_i is the weight fraction, respectively.

The mean free path (Eq. (2)), half-value layer (Eq. (3)), and tenth-value layer (Eq. (4)) parameters are calculated employing the following expressions [14]:

$$\lambda = \frac{1}{\kappa} \tag{2}$$

$$H_{VL} = \frac{\ln(2)}{\kappa} \tag{3}$$

$$T_{VL} = \frac{\ln(10)}{\kappa} \tag{4}$$

where κ is the linear attenuation coefficient.

In this study, the radiation shielding properties of contrasting soils were studied in the 1 keV to 10 MeV energy band. Four photon additional energies were also selected referring to the ^{241}Am (59.5 keV), ^{133}Ba (356 keV), ^{137}Cs (661.6 keV), and ^{60}Co (1.33 MeV) radioactive sources. These radioactive materials can be produced, for example, in underground nuclear explosions. Thus, the soil shielding properties associated with these four-photon energies were also investigated.

The linear attenuation coefficient of the soils was also measured using the gamma-ray attenuation traditional method. The counting sequence by Conner et al. [15] was selected for the measurements due to its low statistical uncertainty. The mass attenuation coefficient was then obtained using information about the density (disturbed samples) of the soils. The ^{241}Am and ^{137}Cs radioactive sources were employed in the experimental measurements. A NaI(Tl) flat solid scintillation detector (7.62 × 7.62 cm) along with standard spectrometric gamma-ray electronics were utilized to detect the photons emitted from the gamma-ray sources [14].

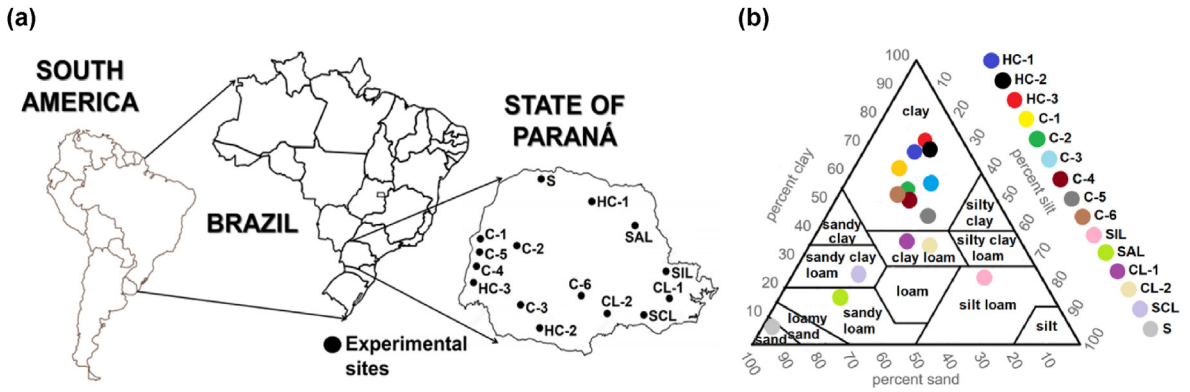

Fig. 1. (a) Location of the experimental sites (tropical/sub-tropical climate) and (b) USDA soil texture triangle presenting the soil types studied. HC: Heavy clay; C: Clay; SIL: Silt loam; SAL: Sandy loam; CL: Clay loam; SCL: Sandy clay loam; S: Sand.

Circular lead collimators presenting diameters of 2 and 4.5 mm were assembled between the radioactive sources and the detector. The distance between them was kept constant (23 cm), and both collimators were adjusted and aligned using a laser point to avoid inappropriate beam geometry. For the experimental evaluation of κ, disturbed soil samples were dried in a forced air circulation oven (105 °C for 24 h) and sieved in a 1 mm mesh sieve. After that, the soil samples were gently packed into a thin wall (0.5 cm) acrylic container (10 × 10 × 10 cm).

The Beer-Lambert law was employed to measure κ through the following equation:

$$k = \frac{1}{x}\ln\left(\frac{I_0}{I}\right) \quad (5)$$

where I is the intensity after transmission through the sample of thickness x and I_0 is the incident photon intensity (on the sample), respectively. Soil density (ρ) was obtained through the relation between the dry soil mass and the internal volume of the acrylic container filled with soil. The relation between κ and ρ was utilized to calculate μ.

The degree of weathering was measured based on the use of Ki and Kr indices, which are calculated as follows [16]:

$$Ki = \left(\frac{\%SiO_2}{\%Al_2O_3}\right) \times 1.70 \quad (6)$$

$$Kr = \frac{\%SiO_2/0.60}{(\%Al_2O_3/1.02) + (\%Fe_2O_3/1.60)} \quad (7)$$

In tropical/sub-tropical soils, the kaolinite molecular ratio (Ki) is the basis to distinguish highly (≤2.2) or poorly (>2.2) weathered soils. The Kr index varies from ≤0.75 (highly weathered soils) to >0.75 (poorly weathered soils), respectively.

Pearson correlation coefficients were calculated to check possible correlations between clay, silt, sand, oxide contents (major oxides), and the radiation shielding parameters (μ, λ, H_{VL}, and T_{VL}). Multiple linear regression analyses were employed to compare the role of the soil composition in the radiation attenuation. All data were analyzed using the software Past [17].

3. Results

The variation of the total and partial mass attenuation coefficients with the photon energy for the contrasting soils is discussed below (Fig. 2). The results demonstrate that μ is dependent on the photon energy and chemical composition of the soils (Fig. 2a). In the soils studied, μ variation with photon energy was almost similar among them (E < 6 keV and E > 0.2 MeV). The main differences noticed at low photon energies, between 6 and 80 keV, were related to Fe_2O_3, TiO_2, and Al_2O_3 amounts found in the soil samples [18]. These three oxides were linearly correlated with μ presenting strong to very strong positive correlations at low photon energies, e.g. 59.5 keV (Al_2O_3: r = 0.78, p < 0.05; Fe_2O_3: r = 0.94, p < 0.05; TiO_2: r = 0.83, p < 0.05). Soils with the highest amounts of these oxides were also those with the highest μ (Table 1). Strong to very strong linear positive correlations were also found between clay × Fe_2O_3 (r = 0.84, p = 0.09), clay × TiO_2 (r = 0.71, p < 0.05), and clay × Al_2O_3 (r = 0.87, p = 0.32) (Table 1). Sand was inversely related to Al_2O_3 (r = −0.61, p < 0.05) and Fe_2O_3 (r = −0.64, p < 0.05). The same trend was observed for SiO_2 × μ and sand × μ at low photon energies, e.g. 59.5 keV (SiO_2: r = −0.93, p < 0.05; sand: r = −0.66, p < 0.05).

Regarding the dominance of the partial photon processes of interaction with the soils (photoelectric absorption – PA; incoherent scattering – IS; pair production at the nuclear field – PP), slight differences were observed for μ among soils in the energy region where photoelectric absorption was dominant (E ≤ 0.1 MeV) (Fig. 2b). For intermediate photon energies (0.1 < E ≤ 1 MeV), the incoherent scattering was predominant over μ as expected (Fig. 2c). At photon energies higher than 1.022 MeV (energy related to two times the electron rest mass), the pair production (nuclear field) started to contribute to μ (Fig. 2d). The soils showing the highest amounts of Fe_2O_3 and TiO_2 were those with the highest μ_{PP} values, which confirms Z^2 dependence on μ for this effect [19]. However, it seems relevant to highlight that the division between low, intermediate, and high photon energies, selected in this study, was based on the dominance of each of the radiation interaction processes (PA, IS, PP) when different energy ranges are analyzed.

To demonstrate the feasibility of the simulated method presented here to analyze the radiation attenuation properties of contrasting soils, the computer-based (XCOM) simulated μ values were compared to the experimental ones at two photon energies: 59.5 keV (^{241}Am) and 661.6 keV (^{137}Cs) (Table 2). The lowest and the highest relative differences (absolute values), between the XCOM and experimental values, were 0.2% (C-4) and 21.0% (C-2) (^{241}Am), and 0.3% (SCL) and 5.3% (C-4) (^{137}Cs), respectively. Difficulties in filling up the acrylic containers, mainly regarding clay soils (composed of small particles – equivalent spherical diameter <2 μm), can explain the highest relative differences observed in this study for some soils. Additionally, the highest differences observed, mainly in relation to low photon energies, can be associated with the nature of the mixture rule, which sometimes disregards interactions amongst the atoms of the compounds [7,20].

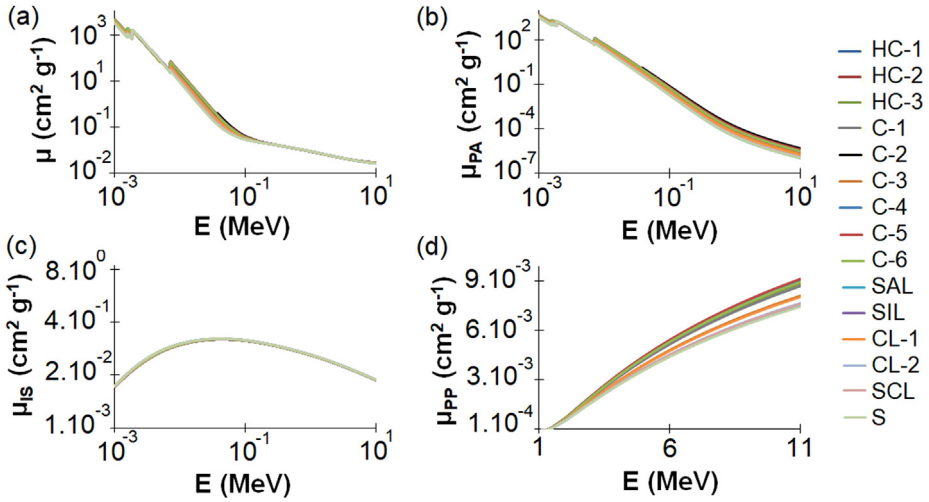

Fig. 2. (a) Simulated total mass attenuation coefficient (μ) variation with photon energy (E), (b) Contribution of the photoelectric absorption (PA) to μ and its variation with E, (c) Contribution of the incoherent scattering (IS) to μ and its variation with E, and (d) Contribution of the pair production (PP) to μ and its variation with E. HC: Heavy clay; C: Clay; SIL: Silt loam; SAL: Sandy loam; CL: Clay loam; SCL: Sandy clay loam; S: Sand.

Table 2
Experimental and theoretical mass attenuation coefficient (μ) and soil density (ρ) of the contrasting soils studied at two photon energies (59.5 and 661.6 keV).

Soil type	Photon energy (keV)				Soil density (g cm^{-3})
	59.5		661.6		
	Meas.	Theor.	Meas.	Theor.	
HC-1	0.4315	0.4473	0.0746	0.0759	0.93
HC-2	0.4079	0.4582	0.0765	0.0759	1.03
HC-3	0.3934	0.4959	0.0780	0.0761	0.97
C-1	0.4148	0.4216	0.0749	0.0760	1.03
C-2	0.4258	0.5391	0.0771	0.0760	0.95
C-3	0.3187	0.3812	0.0792	0.0764	0.96
C-4	0.4630	0.4638	0.0719	0.0759	1.04
C-5	0.4681	0.4934	0.0766	0.0760	1.03
C-6	0.4540	0.4515	0.0779	0.0758	1.08
SIL	0.2753	0.2915	0.0773	0.0769	0.90
SAL	0.2750	0.2812	0.0779	0.0769	1.32
CL-1	0.3151	0.3433	0.0768	0.0766	0.92
CL-2	0.2892	0.2938	0.0784	0.0768	0.89
SCL	0.2790	0.2903	0.0771	0.0769	1.00
S	0.2599	0.2718	0.0781	0.0770	1.27

HC: Heavy clay; C: Clay; SIL: Silt loam; SAL: Sandy loam; CL: Clay loam; SCL: Sandy clay loam; S: Sand.

The results of λ demonstrate that low energy photons lost their energy in shorter distances traveling through the soil than intermediate and high energy photons, as expected (Fig. 3a). For photons with energies of 10 keV and 0.1 MeV (photoelectric absorption dominance maximum energy value), the average distance between successive interactions of photons ranged from 0.019 cm (C-4) to 0.045 cm (CL-2) (10 keV) and from 4.36 cm (SAL) to 6.37 cm (CL-2) (0.1 MeV) (Supplementary Fig. S1). For photons of intermediate energies (incoherent scattering dominance), for example, 1 MeV, the average distance between successive interactions of photons ranged from 11.97 cm (SAL) to 17.77 cm (CL-2) (Supplementary Fig. S1). For high energy photons (nearing pair production dominance), for example, 10 MeV, the average distance between successive interactions of photons ranged from 33.29 cm (SAL) to 49.19 cm (CL-2) (Supplementary Fig. S1).

The linear regression analysis revealed close relationships between λ and the soil parameters clay, Al_2O_3, Fe_2O_3, and TiO_2 contents (Table 1). Moderate to strong linear negative correlations were found between these parameters (λ × clay: $r = -0.67$, $p < 0.05$; λ × Al_2O_3: $r = -0.74$, $p < 0.05$; λ × Fe_2O_3: $r = -0.86$, $p = 0.40$; λ × TiO_2: $r = -0.78$, $p < 0.05$), meaning that increases in these parameters improve the capability of the soil to attenuate radiation. A strong linear negative correlation was found between λ × μ for low photon energies, as observed for 59.5 keV ($r = -0.86$, $p < 0.05$). However, it is important to point out that λ, H_{VL}, and T_{VL} were obtained based on the linear attenuation coefficient, which is highly dependent on the soil density [19,21–23]. It is also worth mentioning that the measured density (Table 2) was obtained for disturbed soil samples, which means that there was no soil structure.

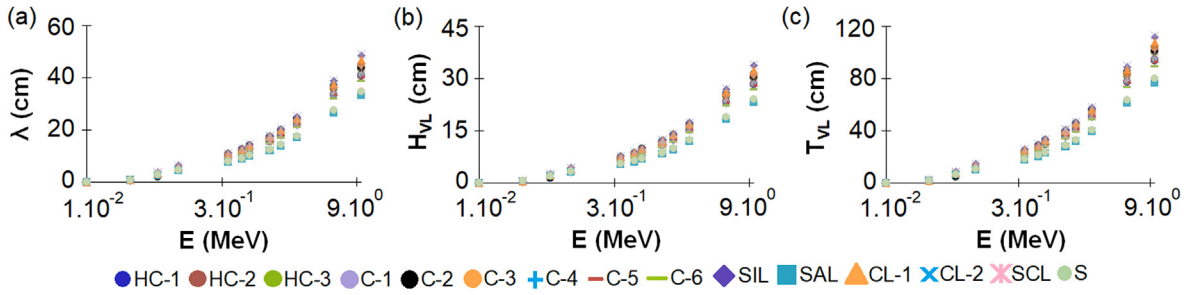

Fig. 3. (a) Mean free path (λ) variation with photon energy (E), (b) Half-value layer (H_{VL}) variation with E, and (c) Tenth-value layer (T_{VL}) variation with E. HC: Heavy clay; C: Clay; SIL: Silt loam; SAL: Sandy loam; CL: Clay loam; SCL: Sandy clay loam; S: Sand.

H_{VL} and T_{VL} parameters (Fig. 3b and c) followed the same trend as that of the results observed for λ based on κ measured (results not shown in Table 2), as expected. Lower H_{VL} and T_{VL} values mean higher efficiency of a specific soil to attenuate the photons. Thus, lower values of these two parameters are an indication of better shielding capabilities. For photons with energies of 10 keV and 0.1 MeV (photoelectric absorption dominance), H_{VL} ranged from 0.013 cm (C-4) to 0.031 cm (CL-2) (10 keV) and from 3.02 cm (SAL) to 4.42 cm (CL-2) (0.1 MeV); while T_{VL} ranged from 0.043 cm (C-4) to 0.103 cm (CL-2) (10 keV) and from 10.04 cm (SAL) to 14.67 cm (CL-2) (0.1 MeV) (Supplementary Figs. S2 and S3). For photons of intermediate energies (incoherent scattering dominance), like those of 1 MeV, H_{VL} ranged from 8.30 cm (SAL) to 12.32 cm (CL-2) (Supplementary Fig. S2), while T_{VL} ranged between 27.56 cm (SAL) and 40.92 cm (CL-2) (Supplementary Fig. S3). For photons of high energy (nearing pair production dominance), like those of 10 MeV, H_{VL} ranged from 23.07 cm (SAL) to 34.10 cm (CL-2) (Supplementary Fig. S2), while T_{VL} ranged from 76.64 cm (SAL) to 113.27 cm (CL-2) (Supplementary Fig. S3), respectively.

Similar to the results of λ, the linear regression analysis revealed close relationships between H_{VL} and T_{VL} and the soil parameters clay, Al_2O_3, Fe_2O_3, and TiO_2 contents (Table 1). Moderate to strong linear negative correlations were found between these parameters (clay: $r = -0.65$, $p < 0.05$; Al_2O_3: $r = -0.74$, $p < 0.05$; Fe_2O_3: $r = -0.86$, $p = 0.40$; TiO_2: $r = -0.79$, $p < 0.05$ for H_{VL} and clay: $r = -0.66$, $p < 0.05$; Al_2O_3: $r = -0.74$, $p < 0.05$; Fe_2O_3: $r = -0.86$, $p = 0.40$; TiO_2: $r = -0.79$, $p < 0.05$ for T_{VL}), which means that increases in these parameters mean better soil shielding capability.

The results observed here indicate that not only do the soil chemical and granulometric compositions influence λ, H_{VL}, and T_{VL}, but their densities also play an important role. For example, at photon energies higher than 0.1 MeV, SAL presented the best shielding properties (λ, H_{VL}, and T_{VL}). This soil has the second smallest clay content and only 24.9% is $Al_2O_3 + Fe_2O_3 + TiO_2$ contents (Table 1). However, SAL presented a 1.32 g cm^{-3} density when packed into the acrylic box (experimental measurement), which was on average 1.3 times higher than the values found for clay soils. It seems important to mention that the soil density affects the measurement of κ directly influencing the values of λ, H_{VL}, and T_{VL} (Eqs. (2)–(4)).

Regarding the indices utilized to infer soil weathering, soils HC and C were seen to present Ki values lower than 2.2. For these soils, Ki values ranged from 0.88 (C-6) to 1.69 (C-4). This is an indication that they are highly weathered. The same result was obtained for Kr with values close to 0.75 for HC and C soils. Kr values ranged from 0.63 (C-6) to 1.20 (C-3) in these soils. The other soils analyzed presented high Ki values (ranging from 4.08 − CL-1 to 7.91 − SIL) and Kr (ranging from 3.11 − CL-1 to 6.76 − SIL), which is an indication of poorly weathered soils. The analysis of correlation showed that both Ki and Kr were inversely related to clay (Ki: $r = -0.91$, $p < 0.05$; Kr: $r = -0.92$, $p < 0.05$), Fe_2O_3 (Ki: $r = -0.90$, $p < 0.05$; Kr: $r = -0.92$, $p < 0.05$), Al_2O_3 (Ki: $r = -0.94$, $p < 0.05$; Kr: $r = -0.93$, $p < 0.05$), and TiO_2 (Ki: $r = -0.84$, $p = 0.91$; Kr: $r = -0.86$, $p = 0.38$) contents. The same behavior was observed for the relation between $\mu \times Ki$ ($r = -0.89$, $p = 0.07$) and $\mu \times Kr$ ($r = -0.91$, $p < 0.05$) at low photon energies (59.5 keV). On the other hand, strong linear positive correlations were found between Ki and Kr and the parameters of radiation shielding λ (Ki: $r = 0.84$, $p < 0.05$; Kr: $r = 0.82$, $p < 0.05$), H_{VL} (Ki: $r = 0.82$, $p < 0.05$; Kr: $r = 0.81$, $p < 0.05$), and T_{VL} (Ki: $r = 0.83$, $p < 0.05$; Kr: $r = 0.82$, $p < 0.05$). This result indicates that weathered soils, considering their chemical and granulometric compositions regardless of the density influence, tend to present the best shielding capabilities.

Fig. 4 shows an analysis of H_{VL} values for different energy ranges considering the distinct radiation interaction processes. At low photon energies ($E \leq 0.1$ MeV), H_{VL} increased rapidly with the energy increase influenced mainly by the photoelectric absorption (Fig. 4a). In the intermediate photon energy range ($0.1 < E \leq 1$ MeV), H_{VL} kept its increasing trend influenced mainly by the incoherent scattering, which presented an interaction cross-section directly proportional to Z (Fig. 4b). Finally, in the high energy range studied ($1 < E \leq 10$ MeV), the pair production cross-section along with the incoherent scattering were responsible for the increase in H_{VL} (Fig. 4c). At energies higher than 0.1 MeV, SAL was the soil with the best shielding properties (lowest slope of the straight lines at all energy ranges studied) (Figs. 3b and 4b,c). The region of high photon energies (Fig. 4c) was the one where SAL showed its best shielding performance when compared to the other soils; mainly influenced by the importance of the incoherent scattering and pair production processes [19].

The values of λ, H_{VL}, and T_{VL} at the photon energies of ^{241}Am, ^{133}Ba, ^{137}Cs, and ^{60}Co radioactive sources for the contrasting soils and lead (Pb) are shown below (Table 3).

Analyzing the results presented in Table 3, the soil with the best shielding properties (SAL) (except for 59.5 keV) showed a difference of c. 25 times for λ, H_{VL}, and T_{VL} when compared to lead at 356 keV (^{133}Ba) photon energy, c. 12 times for 661.6 keV (^{137}Cs), and c. 9 times for 1.33 MeV (^{60}Co). As it is well known, the lead best shielding properties in relation to other materials is mainly related to its high density (c. 11.3 g cm^{-3}). To improve the efficiency of the soil as a shielding material, besides the influence of its composition, one of the best options is to compact this porous material to increase its density. However, for soils with similar densities, those composed of high atomic number elements and high amounts of clay tend to present the best shielding performance. Thus, a combination between soil density and its chemical and granulometric composition will offer the best radiation attenuation.

4. Discussion

The results presented in this study showed the importance of the granulometric soil fractions, especially clay content, and the main soil oxides (Al_2O_3, Fe_2O_3, TiO_2, and SiO_2) in the attenuation of radiation [18]. As expected, increased photon energy caused decreases in μ (Fig. 2). The mass attenuation coefficient decreases sharply at low photon energies ($E \leq 0.1$ MeV), which is mainly associated with the dominance of the photoelectric absorption when compared to the other processes [19,23–25]. The cross-section of the photoelectric absorption is inversely related to the photon energy ($E^{3.5}$) and directly proportional to the atomic number (Z^{4-5}) [19]. The differences observed in the chemical composition of the soils explain the differences observed in μ, mainly at low photon energies (Tables 1 and 2). The several jumps at energies lower than 0.01 MeV are related to the K-edge absorption for the high atomic number compounds (Fig. 2). At intermediate photon energies ($0.1 < E \leq 1$ MeV), μ decreased slowly with the increased incident photon energy, which occurs due to the incoherent scattering dominance. However, no differences were observed among the soils due to the linear dependency of this effect with Z. As for the incoherent scattering, the number of electrons per gram is the most important factor in the photon interaction with the soil [19]. Finally, in the high energy region ($E > 1$ MeV), pair production along with incoherent scattering were the most important processes contributing to the radiation attenuation (Fig. 2). The increases observed in μ with the photon energy for the pair production were associated with the Z^2 dependence on its cross-section [19,23].

The results of μ for the contrasting soils showed the importance of their chemical composition in the radiation attenuation [26]. For the weathered soils studied, the ones containing high atomic

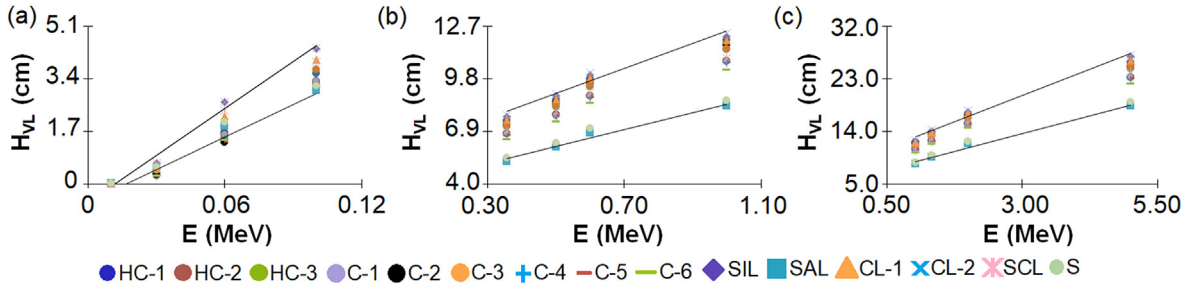

Fig. 4. Half-value layer (H_{VL}) variation with energy (E). (a) $0.01 \leq E \leq 0.1$ MeV, (b) $0.1 < E \leq 1$ MeV, and (c) $1 < E \leq 5$ MeV. HC: Heavy clay; C: Clay; SIL: Silt loam; SAL: Sandy loam; CL: Clay loam; SCL: Sandy clay loam; S: Sand.

Table 3
Mean free path (λ), half-value layer (H_{VL}), and tenth-value layer (T_{VL}) for the contrasting soils studied and photon energies of interest in the soil science.

Soil type/Material	Shielding property (cm)/Photon energy (keV)											
	59.5			356			661.6			1330		
	λ	H_{VL}	T_{VL}	λ	H_{VL}	T_{VL}	λ	H_{VL}	T_{VL}	λ	H_{VL}	T_{VL}
HC-1	2.4	1.7	5.5	10.8	7.5	24.9	14.2	9.8	32.6	19.9	13.8	45.8
HC-2	2.1	1.5	4.9	9.7	6.8	22.4	12.8	8.9	29.4	18.0	12.5	41.4
HC-3	2.1	1.4	4.8	10.3	7.1	23.7	13.6	9.4	31.2	19.1	13.2	43.9
C-1	2.3	1.6	5.3	9.8	6.8	22.5	12.8	8.9	29.4	17.9	12.4	41.3
C-2	2.0	1.4	4.5	10.5	7.3	24.2	13.9	9.6	31.9	19.5	13.5	44.9
C-3	2.7	1.9	6.3	10.4	7.2	24.0	13.6	9.5	31.4	19.1	13.3	44.1
C-4	2.1	1.4	4.8	9.7	6.7	22.2	12.7	8.8	29.2	17.8	12.3	41.0
C-5	2.0	1.4	4.5	9.7	6.7	22.4	12.8	8.9	29.4	18.0	12.5	41.4
C-6	2.1	1.4	4.7	9.3	6.5	21.4	12.2	8.5	28.1	17.2	11.9	39.5
SIL	3.8	2.6	8.8	11.1	7.7	25.6	14.4	10.0	33.3	20.3	14.0	46.7
SAL	2.7	1.9	6.2	7.6	5.2	17.4	9.9	6.8	22.7	13.8	9.6	31.8
CL-1	3.2	2.2	7.3	10.9	7.5	25.1	14.2	9.8	32.7	19.9	13.8	45.9
CL-2	3.8	2.7	8.8	11.2	7.8	25.9	14.6	10.1	33.7	20.5	14.2	47.2
SCL	3.4	2.4	7.9	10.0	6.9	23.0	13.0	9.0	30.0	18.2	12.6	42.0
S	2.9	2.0	6.7	7.9	5.5	18.1	10.2	7.1	23.6	14.3	9.9	33.0
Lead	0.02	0.01	0.04	0.3	0.2	0.7	0.8	0.6	1.9	1.6	1.1	3.6

The parameters λ, H_{VL}, and T_{VL} are expressed in centimeters (cm). HC: Heavy clay; C: Clay; SIL: Silt loam; SAL: Sandy loam; CL: Clay loam; SCL: Sandy clay loam; S: Sand.

elements (e.g. Fe_2O_3 + TiO_2) were also the soils with the highest attenuation capacity (Tables 1 and 2), mainly at low photon energies [14,26,27], corroborated by linear relations between the oxides Fe_2O_3 and TiO_2, and μ [14]. Similar findings were observed for the relation between clay content and μ (Tables 1 and 2), which was associated with the composition of clayey soils. Soils in tropical/sub-tropical regions are composed of several types of minerals (mainly secondary minerals) having different chemical compositions and densities with important influence in radiation interaction processes as evidenced in this research [9,28,29]. Thus, the variations in μ observed among soils, in the region of the photoelectric absorption and pair production dominance, were related to the differences in the soil chemical composition and the cross-section dependence on Z for these two processes [21,30].

The radiation shielding parameters (λ, H_{VL}, and T_{VL}) were also influenced by the granulometric fractions of the soils, especially clay content and the soil chemical compositions (Fig. 3, Supplementary Figs. S1–S3). As already mentioned, increases in the clay, Al_2O_3, Fe_2O_3, and TiO_2 contents caused reductions in λ, H_{VL}, and T_{VL}, demonstrating the effectiveness of these properties to attenuate radiation. Low values of these parameters mean that small thicknesses are necessary for shielding the radiation at specific photon energies [31]. Another finding was that λ, H_{VL}, and T_{VL} values are low at lower photon energies (photoelectric absorption region) gradually increasing at intermediate (incoherent scattering region) and high photon energies (pair production region) (Fig. 3, Supplementary Figs. S1–S3) [6]. Despite the importance of the granulometric soil fractions and the chemical composition to the radiation attenuation, the density of the soils also plays an important role in their shielding properties [1,5,32–34]. In this study, for example, the sandy loam and sand soils presented densities c. 1.3 times higher than the other soils (Table 2), influencing their values of κ and, consequently, λ, H_{VL}, and T_{VL} values (simulated through XCOM) (Table 3).

One of the purposes of this study was to present an analysis of the radiation shielding capability of contrasting weathered soils. The soil chemical composition and the granulometric soil fractions have great importance in radiation attenuation, influenced mainly by the degree of soil weathering. Density is another property that influences the soil radiation shielding properties (λ, H_{VL}, and T_{VL}). The results demonstrated that the contrasting soils present interesting shielding capabilities varying as a function of several parameters such as their chemical composition; demonstrating that the soil origin is important to explain the attenuation ability of the soils. Thus, this study showed the influence of contrasting soil compositions in the radiation attenuation and its variation as a function of the photon energy. However, a limited number of soil types was evaluated in this study, which means that for a better understanding of the shielding capability of weathered soils, increasing the number of soils investigated might be advisable. It is also important to include other soil properties such as bulk density, total porosity, structure, etc. Finally, the neutron shielding effectiveness (not covered in this study) might also be another interesting subject for future studies aiming to

check the potential application of weathered soils in radiation shielding.

5. Conclusions

This study focused on the influence of contrasting soil types (different degrees of weathering), presenting distinct densities, clay, silt, sand, and oxide contents, in parameters of the radiation interaction (mass attenuation coefficient, mean free path, half-value layer, and tenth-value layer) aiming at the use of this material for radiation shielding purposes. The results showed that μ decreases rapidly with photon energy due to the influence of the photoelectric absorption at low photon energies. At intermediate and high photon energies, the incoherent scattering and pair production became the predominant radiation interaction effects in all soils. Pair production was the process that allowed better discrimination of partial μ among soils (E > 5 MeV). Clay soils (high Fe_2O_3 and TiO_2 amounts) showed the highest μ_{PP}, mainly influenced by the Z^2 dependence of the pair production at the nuclear field.

Concerning λ, H_{VL}, and T_{VL}, the sandy loam soil presented the lowest values of all these parameters, which demonstrated that this soil was the most effective for radiation shielding purposes (photon energies larger than 0.1 MeV). However, this result was mainly achieved due to the high density of the sandy loam soil analyzed. On the other hand, the clay loam was the soil with the highest λ, H_{VL}, and T_{VL} values. Although the clay loam presented similar chemical composition to that of the sandy loam, its density was c. 1.5 times lower than the latter, influencing its shielding properties. This result reinforces the importance of the density of the soil to influence radiation penetration through this material.

Funding

Brazilian National Council for Scientific and Technological Development (CNPq) through Grant 304925/2019-5 (Productivity in Research).

Availability of data and material

Under request.

Code availability

Not applicable.

Authors' contributions

L.F. Pires: Conceptualization, Data Curation, Writing – Original Draft.

Declaration of competing interest

The authors declare that they have no known competing financial interests or personal relationships that could have appeared to influence the work reported in this paper.

Acknowledgements

Luiz F. Pires would like to acknowledge the financial support provided by the Brazilian National Council for Scientific and Technological Development (CNPq) through Grant 304925/2019-5 (Productivity in Research).

Appendix A. Supplementary data

Supplementary data to this article can be found online at https://doi.org/10.1016/j.net.2022.04.002.

References

[1] A.H. Al-khawlany, A.R. Khan, J.M. Pathan, Investigation of radiation shielding properties for some soil samples for use in shields against gamma-rays from different nuclides, Bull. Pure Ap. Sci. 38 (2019) 32–45.
[2] S.V. Mamikhin, D.V. Manakhov, A.I. Shcheglov, E.V. Tsvetnov, Some aspects of evaluation of the role of soils as a shielding medium from ionizing-radiation, Moscow Univ. Soil Sci. Bull. 72 (2017) 66–70.
[3] S. Gedik, A.F. Baytas, Shielding of gamma radiation by using porous materials, Acta Phys. Pol. 128 (2015) 174–175.
[4] J. Miller, L. Taylor, C. Zeitlin, L. Heilbronn, S. Guetersloh, M. DiGiuseppe, Y. Iwata, T. Murakami, Lunar soil as shielding against space radiation, Radiat. Meas. 44 (2009) 163–167.
[5] E. Yoshikawa, H. Komine, S. Goto, Y. Saito, The evaluation for radiation shielding ability of the soil materials and application to design for construction, in: Proceedings of the 19th International Conference on Soil Mechanics and Geotechnical Engineering, Seoul, 2017.
[6] V.P. Singh, N.M. Badiger, N. Kucuk, Gamma-ray and neutron shielding properties of some soil samples, Indian J. Pure Appl. Phys. 52 (2014) 579–587.
[7] F.C. Hila, G.P. Dicen, A.M.V. Javier-Hila, A. Asuncion-Astronomo, N.R.D. Guillermo, R.V. Rallos, I.A. Navarrete, A.V. Amorsolo Jr., Determination of photon shielding parameters for soils in Mangrove Forests, Philipp. J. Sci. 150 (2021) 245–256.
[8] A.C. Scheinost, Metal Oxides, Encyclopedia of Soils in the Environment, Elsevier, Amsterdam, 2005.
[9] D. Hillel, Environmental Soil Physics, first ed., Academic Press, San Diego, 1998.
[10] T.R. Ferreira, L.F. Pires, A.M. Brinatti, A.C. Auler, Surface liming effects on soil radiation attenuation properties, J. Soils Sediments 18 (2018) 1641–1653.
[11] I.M. Nikbin, R. Mohebbi, S. Dezhampanah, S. Mehdipour, R. Mohammadi, T. Nejat, Gamma ray shielding properties of heavy-weight concrete containing Nano-TiO_2, Radiat. Phys. Chem. 162 (2019) 157–167.
[12] G.W. Gee, J.W. Bauder, Particle-size analysis, in: A. Klute (Ed.), Methods of Soil Analysis, Part I. Physical and Mineralogical Methods, SSSA Book Series, Madison, 1986, pp. 381–411.
[13] M.J. Berger, J.H. Hubbell, S.M. Seltzer, J. Chang, J.S. Coursey, R. Sukumar, D.S. Zucker, K. Olsen, XCOM: Photon Cross Section Database (Version 1.5), National Institute of Standards and Technology, Gaithersburg, MD, 2010 (Online) Available: http://physics.nist.gov/xcom.
[14] M.E. Medhat, L.F. Pires, R.C.J. Arthur, Analysis of photon interaction parameters as function of soil composition, J. Radioanal. Nucl. Chem. 300 (2014) 1105–1112.
[15] A.L. Conner, H.F. Atwater, E.H. Plassmann, J.H. McCrary, Gamma-ray attenuation-coefficient measurements, Phys. Rev. 1 (1970) 539–544.
[16] Embrapa, Manual de métodos de análise do solo, 2ª edição, Centro Nacional de Pesquisa de Solos, Rio de Janeiro, 1997.
[17] O. Hammer, D.A.T. Harper, P.D. Ryan, PAST: paleontological statistics software package for education and data analysis, Paleontol. Electron. 4 (2001) 1–9.
[18] M.S. Al-Masri, M. Hasan, A. Al-Hamwi, Y. Amin, A.W. Doubal, Mass attenuation coefficients of soil and sediment samples using gamma energies from 46.5 to 1332 keV, J. Environ. Radioact. 116 (2013) 28–33.
[19] I. Kaplan, Nuclear Physics, first ed., Addison-Wesley Publishing Company, Cambridge, 1963.
[20] T.A. Almeida Junior, M.S. Nogueira, V. Vivolo, M.P.A. Potiens, L.L. Campos, Mass attenuation coefficients of X-rays in different barite concrete used in radiation protection as shielding against ionizing radiation, Radiat. Phys. Chem. 140 (2017) 349–354.
[21] E.S.B. Ferraz, R.S. Mansell, Determining Water Content and Bulk Density of Soil by Gamma-Ray Attenuation Methods, IFAS, Flórida, 1979, p. 51. Technical Bulletin, No. 807.
[22] L.F. Pires, Soil analysis by nuclear techniques: a literature review of the gamma ray attenuation method, Soil Till. Res. 184 (2018) 216–234.
[23] N. Kucuk, Z. Tumsavas, M. Cakir, Determining photon energy absorption parameters for different soil samples, J. Radiat. Res. 54 (2013) 578–586.
[24] X.-D. Su, G.-L. Zhang, S.-P. Xu, W.-W. Qu, Y.-H. Huang, B. Wang, Y.-F. Wang, Z.-T. Zhang, W.-F. Xu, M.-L. Wang, Attenuation coefficients of gamma and X-rays passing through six materials, Nucl. Sci. Tech. 31 (2020) 3.
[25] F.C. Hila, A.M.V. Javier-Hila, M.I. Sayyed, A. Asuncion-Astronomo, G.P. Dicen, J.F.M. Jecong, N.R.D. Guillermo, A.V. Amorsolo Jr., Evaluation of photon radiation attenuation and buildup factors for energy absorption and exposure in some soils using EPICS2017 library, Nucl. Eng. Technol. 53 (2021) 3808–3815.
[26] C.R. Appoloni, E.A. Rios, Mass attenuation coefficients of Brazilian soils in the range 10-1450 keV, Appl. Radiat. Isot. 45 (1994) 287–291.
[27] M.E. Medhat, Application of gamma-ray transmission method for study the properties of cultivated soil, Ann. Nucl. Energy 40 (2012) 53–59.
[28] W. Chesworth, Soil Mineralogy, first ed., Springer, Dordrecht, 2008.
[29] L.V. Prandel, N.M.P. Dias, S.C. Saab, A.M. Brinatti, N.F.B. Giarola, L.F. Pires, Characterization of kaolinite in the hardsetting clay fraction using atomic

force microscopy, X-ray diffraction, and the Rietveld method, J. Soils Sediments 17 (2017) 2144–2155.
[30] Y. Elmahroug, B. Tellili, C. Souga, Determination of total mass attenuation coefficients, effective atomic numbers and electron densities for different shielding materials, Ann. Nucl. Energy 75 (2015) 268–274.
[31] N. Jamal AbuAlRoos, M.N. Azman, N.A.B. Amin, R. Zainon, Tungsten-based material as promising new lead-free gamma radiation shielding material in nuclear medicine, Phys. Med. 78 (2020) 48–57.
[32] A. Ün, D. Demir, Y. Sahin, Determination of density and volumetric water content of soil at multiple photon energies, Radiat. Phys. Chem. 80 (2011) 863–868.
[33] J.C. Costa, J.A.R. Borges, L.F. Pires, Soil bulk density evaluated by gamma-ray attenuation: analysis of system geometry, Soil Till. Res. 129 (2014) 23–31.
[34] V.N. Ba, B.N. Thien, T.T.H. Loan, Effects of element composition in soil samples on the efficiencies of gamma energy peaks evaluated by the MCNP5 code, Nucl. Eng. Technol. 53 (2021) 337–343.